Phiri, Josphat; Gane, Patrick; Maloney, Thad C.

Multidimensional Co-Exfoliated Activated Graphene-Based Carbon Hybrid for Supercapacitor Electrode

Published in:
Energy Technology

DOI:
10.1002/ente.201900578

Published: 01/01/2019

Document Version
Peer-reviewed accepted author manuscript, also known as Final accepted manuscript or Post-print

Multidimensional co-exfoliated activated graphene-based carbon composite for supercapacitor electrode

Josphat Phiri; Patrick Gane; Thad C. Maloney

Josphat Phiri; Prof. Patrick Gane; Prof. Thad C. Maloney
School of Chemical Engineering, Department of Bioproducts and Biosystems, Aalto University, P.O. Box 16300, 00076 Aalto, Finland
Email: josphat.phiri@aalto.fi; patrick.gane@aalto.fi; thaddeus.maloney@aalto.fi

Keywords: graphene; nano- microfibrillated cellulose; supercapacitors; electrode; activated carbon

Abstract

Herein, we report a simple route for fabrication of highly porous activated few-layer graphene for application in supercapacitors as electrode material. The process makes use of natural and renewable materials which is an essential prerequisite, especially for large scale application. Few-layer graphene is exfoliated in aqueous suspension with the aid of microfibrillated cellulose, an environmentally benign eco-friendly medium that is low-cost, biodegradable and sustainable. The exfoliated product is subsequently activated to increase the surface area and to form the desired pore structure. The prepared electrode materials exhibit a high surface area of up to 720 $m^2 g^{-1}$. We also use microfibrillated cellulose as a non-toxic environmentally friendly binder in the electrode application. The electrochemical performance was evaluated in a three-electrode system and the prepared samples showed a high specific capacitance of up to 120 F g^{-1} at a current density of 1 A g^{-1}. The samples also exhibit a high capacity retention rate of about 99 % after 5 000 cycles and 97 % after 10 000 cycles. The proposed method for

This article has been accepted for publication and undergone full peer review but has not been through the copyediting, typesetting, pagination and proofreading process, which may lead to differences between this version and the Version of Record. Please cite this article as doi: 10.1002/ente.201900578

fabrication of graphene-based supercapacitor electrode material, based largely on renewable and sustainable materials, offers potential for commercially viable application.

1. Introduction

The need for renewable and sustainable energy has become of even greater importance in recent years due to the growing energy demand and ecological concerns such as climate change. Supercapacitors, also called electric double layer capacitors or ultracapacitors, are energy storage devices that store electrical energy in an electrochemical double layer that is formed at the interface between the electrode and electrolyte, and is able to deliver that stored energy at an extremely high rate. In comparison to conventional capacitors, supercapacitors are generally more efficient and have high capacitance values, longer lasting cyclability, low maintenance, wide temperature working range and extremely high charge-discharge cycles [1]. Due to their ability to release energy quickly, supercapacitors are ideal for application where quick energy bursts are required, such as in electronic devices, fuel cells, hybrid vehicles, backup power systems etc. [2].

The electrode is one of the most important parts of supercapacitors. The performance of supercapacitors is hugely affected by the type of electrode material [3]. Some electrode materials that are commonly used include conductive polymers (polyaniline, polypyrrole) [4, 5], metal oxides (MnO_2, NiO) [6-8] and carbon-based materials (activated carbon, graphene, carbon nanotubes etc.) [9-13]. Metal oxides are used due to low resistance and high specific capacitance and whilst, as with conducting polymers, reduction and oxidation processes are responsible for the storage of charge [14]. In commercially available supercapacitors, activated carbon (AC) is typically used due to low cost and high surface area. The main limiting factor for achieving the highest specific capacitance for activated carbon electrodes is the limited accessibility of the electrolyte ions to all the carbon atoms [13]. Moreover, low electrical conductivity of activated carbon limits the application in high power density devices [15]. In the last

two decades or so, carbon nanotubes (CNT) have also been extensively investigated for application in supercapacitors [16, 17]. However, CNT have not reached the promised potential in terms of applications and performance due to high production cost and observed high resistance between the electrode and current collector [15, 16, 18].

In recent years, graphene has emerged as a unique 2-dimensional technological material that has huge technical potential for application as electrode material in supercapacitors due its superlative properties, such as extremely high electrical conductivity, large surface area and excellent chemical stability and mechanical properties [19-21]. Unlike CNT and AC, the effective surface area of graphene does not depend on the pore distribution in the solid state, but rather on the number of graphene layers. A single graphene layer has a theoretical surface area of 2 600 $m^2 g^{-1}$ and if the entire area is utilised, graphene based supercapacitors are capable of reaching specific capacitance values as high as 550 F g^{-1} [22]. However, despite all the excellent properties, graphene fabrication especially for large scale application is still the biggest challenge. Graphene is commonly produced by chemical oxidation of graphite. Large scale application, however, is still problematic due to the negative ecological effect from the traditional synthesis processes and toxic raw materials used in these process. Moreover, the harsh chemical treatment also introduces defects in graphene structure that leads to deterioration of the excellent graphene properties.

For high performance energy storage devices, electrodes are required to have excellent electrical and thermal conductivity, interconnected micro- and mesopores and good mechanical properties.[23] Unfortunately, none of the individual carbon-based electrode materials can meet these requirements. In order to overcome some of the limitations from these individual components, sp^2 hybrid carbon structures have been synthesized. For example, graphene and CNT can provide excellent electrical and mechanical properties but limited surface area and accessible pores mostly due to aggregation whilst activated carbons offer high surface area and abundant pore volume with a well-structured micro- and mesoporous network but poor electrical conductivity. These hybrid structures can be tailored during synthesis to supplement the limitations of each other

[24, 25]. For instance, hydrothermal prepared CNT/carbon composites [26], CNT/activated carbon blends [27], 3D graphene based framework [28] etc., have been used to fabricate high performance electrode materials for energy storage devices with superior electrochemical performance. The homogeneous distribution of sp^2 nanocarbons in the carbon matrix is essential in achieving the desired properties and generally requires one carbon phase to self-organize into the other carbon matrix or scaffold. The synthesis of hybrid structures with dispersed nanocarbons into a well–designed and structured carbon matrix is vital in achieving the excellent electrochemical properties required to meet the growing high performance demand. However, the construction of these high performance carbon hybrid based electrodes is still a big challenge.

In the present study, we aimed to develop a novel and simple route for fabrication of few-layer graphene based composites for supercapacitor electrode application based largely on renewable materials. We showed in our earlier study that few-layer graphene sheets can be directly exfoliated from graphite in microfibrillated cellulose (MFC) suspension by high shear exfoliation [29]. MFC is renewable, biodegrade and sustainable and has a high potential for large scale application. MFC in aqueous suspension was also used as a binder for the electrode fabrication, which is more ecologically friendly in comparison to commonly used highly toxic binders such as poly(vinylidene fluoride) or poly(tetrafluoroethylene) and solvents such as N-Methyl-2-pyrrolidone. We show in this study that this simple and yet ´green` approach for the synthesis of graphene/activated carbon after co-exfoliation of graphene in MFC suspension, can be used to synthesise high performance composites for supercapacitor electrode with high scalability potential.

2. Results and discussion

The general synthesis route of graphene/AC composite is schematically illustrated in **Figure 1**. Briefly, natural graphite was added into MFC suspension at a predetermined range of concentrations and subjected to high shear exfoliation [29]. The exfoliated few-layer graphene sheets together with MFC fibres were then activated with KOH at 800 °C for 1 h.

Scanning electron microscopy (SEM) was employed to study the morphologies of the samples (**Figure 2 and 3**). A porous structure with big pores is observed for G0-0% with quite smooth surfaces. However, a three-dimensional porous hierarchical structure is observed for samples with 5 % graphene, as shown in **Figure 3.** A randomly interconnected porous network with varying pore sizes is revealed in the magnified SEM image in **Figure 2b**, showing that the graphene/carbon skeleton is formed around the pores to create a randomly porous multidimensional structure, very similar to that previously observed in activated carbon [30]. The addition of 5 % graphene led to a well-developed pore structure and enhanced surface area which is expected to increase the ionic transfer within the porous carbon network and, thus, improve the electrochemical performance [31]. At high graphene concentration of 10 % (Figure 2c), a more densely packed structure is observed with less cavities than those observed in G1-5%. At 15 % (Figure 2d), small clumps and agglomerates are visible throughout the structure and this is likely attributed to the agglomeration of graphene. Chemical activation, with KOH for example, is widely implemented for the fabrication of highly porous activated carbon/graphene-based composites [32]. KOH is believed not only to digest the graphene/activated carbon composites but also plays a significant role in reorganization into highly porous hierarchical structure [33].

Raman spectroscopy is the most used non-destructive method for characterization of the structure and quality of carbon based materials, particularly to determine the degree of defects and disorder. In **Figure 4a**, the Raman spectra show that all graphene doped samples display the three dominant bands, D-band (~1 540 cm^{-1}), G-band (~1 567 cm^{-1}) and 2D-band

(~2 678 cm^{-1}), commonly present in graphene. However, for the reference sample without graphene, the 2D is not visible. The G-band is related to the relative vibration of the ordered sp^2 bonded carbon atoms, while the D-band is due to the ring breathing modes and arises due to defects and disorder in carbon atoms [34]. The 2D band is the second order of the D-band, and its presence is not dependent on defects and is always present even in pristine graphene. The shape and position of the 2D-band in all prepared samples is consistent with that of few-layer graphene sheets [35]. The I_D/I_G intensity ratio is a used to estimate the quantity or degree of disorder and defects. The reference sample showed a high degree of disorder as evident by the high I_D/I_G ratio, indicating a lower degree of graphitisation than all the graphene doped samples which showed a very low degree of disorder as shown by low I_D/I_G ratio in **Table 1**.

XPS analysis was used to study the surface chemistry of the samples. The XPS wide scans are shown in Figure 4b. The pronounced peaks with binding energies at around 284.8 and 533 eV are assigned to the elements C and O, respectively. The exact composition is shown in Table 1, and it is evident that almost no inorganic impurities are detected in any of the samples. Generally, the amount of graphene added in the samples did not have much effect on the chemical composition of the samples. The C1s for the pure carbonised MFC fibres shown in Figure 4c can be fitted by three components corresponding to C-C, C-O and C=O functional groups [36]. However, with the addition of graphene, the high resolution C1s spectra (Figure 4d-f) showed that all samples consist of four main groups. The peaks at binding energies of around 284.8, 285.5, 286.4 and 287.6 eV corresponding to C=C, C-C, C-O and C=O groups, respectively [37, 38]. It can also be seen that all the samples are dominated by the sp^2 hybridised carbon atoms, evident by the large area occupied as identified C=C atoms [39]. The oxygen containing functional groups present in all the samples can aid in the wettability of the electrodes especially in aqueous based electrolyte which can lead to enhanced capacitive performance [36]. Moreover, heteroatoms such as oxygen can provide pseudocapacitance which can lead to an overall increase of effective capacitance.

The capacitance of supercapacitors is greatly dependent on the surface are and pore structure of the electrode materials. The pore structure of the samples was analysed by N_2 sorption measurements at 77 K (**Figure 5**). The nitrogen isotherm in Figure 5a for all the samples shows a typical International Union of Pure and Applied Chemistry (IUPAC) type-IV isotherm curve with a well-pronounced hysteresis in the $p/p°$ region of around 0.4-1.0, indicating the presence of mesopores. Besides, the steep increase of adsorbed nitrogen at low relative pressure indicates the presence of microspores. The Brunauer- Emmett- Teller (BET) specific surface area (SSA) of G1-5% is ~720 $m^2 g^{-1}$ whilst for G2-10% and G3-15% is ~546 and ~424 $m^2 g^{-1}$, respectively. When the amount of graphene is increased, the distances between the graphene flakes are reduced, which, in turn, leads to a high overall intensity of the van der Waals forces acting between the graphene particles and, thus, high graphene aggregation. These results are in agreement with what was observed in SEM and Raman analyses. The electrochemical performance of carbon-based supercapacitors is greatly affected by the pore structure profiles. Micropores are considered to have a great effect on the specific capacitance [1, 40], whilst the mesopores are thought to have a big influence on capacitance retention especially at high scan rates [41]. The pore size distribution (PSD) and cumulative pore volume of the samples are shown in Figure 5b and c, and **Table 2** shows some pore size characteristics. The PSD for G1-5% is dominated by both micro- and mesopores and peaks at 1.58 nm. As the concentration of graphene is increased, the peak is shifted to bigger pore width, i.e. 1.69 and 2.66 nm for G2-10% and G3-15%, respectively. Moreover, at high graphene concentration, the composites consist of a wide range of PSD comprising a high amount of meso- and macrospores.

The electrochemical performance testing of the samples was conducted in a three-electrode system by using 6 M KOH aqueous solution as the electrolyte. Cyclic voltammetry (CV), galvanostatic charge-discharge and electrochemical impedance systems were employed for the analysis. The CV of the samples is shown in **Figure 6a**, **c** and **e**. The measurements were performed at room temperature within the potential window of 0 to -1 V. The shape for all three samples showed a typical rectangular form at all different sweep rates indicating excellent reversible electric double-layer capacitive behaviour [42]. Moreover, the absence of Faradic peaks also indicate the excellent capacitive charging and discharging behaviour with small equivalent series resistance and good electrochemical performance [43]. This behaviour was observed for all samples at various scan rates. It is also important to note that the broader voltammogram area observed for G1-5% indicates that it has a much more efficient cycle reversibility and higher electrical double layer capacitance during the charge/discharge cycles compared to samples G2-10% and G3-15%.

The galvanostatic charge/discharge cycles (GCD) curves for all samples at different scan rates are shown in Figure 6b, d and f. All the charge-discharge curves show a similar symmetrical triangular curve which is a typical charge/discharge characteristic of carbon-based electrical double-layer capacitators. A sharp and sudden initial potential drop (known as *iR* drop) is usually seen at the start of current discharge in electro double layer capacitors. This *iR* drop is caused by high electrolyte resistance and limited diffusion mobility of electrolyte ions in the electrode. The *iR* drop is virtually negligible in the prepared samples, showing that they have a very high rate of ion transfer inside and between the electrode and electrolyte. Furthermore, when comparing the three samples, the discharge slope of G1-5% at all current densities showed a straight line which indicates excellent stability and discharge properties [44]. Moreover, G1-5% also shows significantly longer charge-discharge times at the same current density in comparison to G2-10% and G3-15%, indicating higher capacitance and more efficient charge/discharge cycles caused by the higher number of

electrons and ions rapidly transferring between the electrolyte and electrode. The linear and symmetrical charge/discharge curves observed even at very high current density also indicate the excellent electrochemical reversibility and very low voltage drop at the start of the discharge curve. In contrast, both G2-10% and G3-15% showed non-linear discharge curves at all current densities, being more pronounced at high current densities. This shows that at high graphene loading, there is a poor electrochemical reversibility caused by the low specific surface area and poorly formed pore structure caused by high concentration of graphene aggregation and, thus, poor electron and ion exchange between the electrolyte and electrode.

Figure 7a shows the specific capacitance of the samples calculated from the discharge curves obtained at current densities ranging from 0.5 to 10 A g^{-1}. The decrease of specific capacitance is usually observed with an increase in current density due to the internal resistance of the electrode. G1-5% samples exhibit a high specific capacitance of 120 F g^{-1} at 1 A g^{-1} which decreases to 102 F g^{-1} at 10 A g^{-1} (85 % retention). However, for the G2-10% and G3-15%, 80 % and 69 % retentions are observed, respectively. The high retention of the G1-5% can be ascribed to low internal resistance, high surface area and well-developed porosity that leads to superior high-rate charge/discharge capability, which is in agreement with the BET measurements.

The electrochemical performance of the prepared electrodes was also analysed by electrochemical impedance spectroscopy (EIS). Figure 7b shows the Nyquist plot measured in the frequency range of 0.01 Hz to 1 MHz, where the Z' axis displays the real part representing ohmic resistance while Z'' the imaginary part represents the presence of non-resistive elements [45]. The Nyquist plot for all the three samples reveals three main segments. The first segment is the vertical line in the low frequency region. This represents the dominance of capacitive behaviour of the electrode [46, 47]. The G1-5% shows more capacitive behaviour

than the other two samples, as shown by the vertical line being more parallel to the imaginary axis. The second segment is the part of the curve having a slope of 45° in the middle frequency range, also known as Warburg resistance, represents ion diffusion and transport between the electrolyte and electrode [48]. Interestingly, the G1-5% has a shorter ion diffusion path than that of G2-10% and G3-15%, which allows easy access and rapid transfer of ions in and out of the electrode and, thus, leads to a higher capacitance. The third segment consists of a depressed semicircle or arc in the high frequency region. This is related to the faradic charge transfer resistance of the electrode and its pore structure. The lack of a more pronounced semicircle represents the low resistance of the electrodes. However, G1-5% shows the smallest arc indicating the smallest charge transfer resistance. This indicates a well-developed pore structure as earlier indicated by SEM and BET analyses. The semicircle radii of G2-10% and G3-15% are very similar and much larger than G1-5%, which indicates high resistance. Furthermore, the intersection with the *x*-axis in the high frequency region represents the equivalent series resistance (ESR) of the supercapacitors [49]. ESR can be used to determine the rate capability of the charge-discharge cycles of the supercapacitors. The ESR also shows electron conduction and ionic transport resistance within the electrode and to and from the electrolyte [50]. For samples G1-5%, G2-10% and G3-15%, the ESR is determined to be 0.219, 0.393 and 0.481 Ω, respectively, which is relatively low. The range of the values is typical for carbon-based supercapacitors, as reported earlier [50, 51]. It is important to note that the resistance is increasing with increase in graphene content. This is probably due to graphene aggregation which prevents the formation of a continuous network. The results are in agreement with what was observed in SEM and Raman analyses.

High stability and durability of electrode materials is required to ensure long term and high efficient operation. GCD was employed to study the stability of the electrode material (G1-5%) by constant charge-discharge cycles. As shown in **Figure 8**, the G1-5% electrode was tested at 5 000 cycles at the constant current density of 5 A g^{-1}. The insert

shows the charge-discharge cycles at the beginning and end cycles. It is clear that the shape is not altered, indicating excellent stability of the electrode. After 5 000 cycles, the electrode retained 99.1 % of the initial capacitance, showing an excellent electrochemical stability rate and cycling reversibility. It is important to note that the slightly lower capacitance retention (~98 %) is observed after the initial 1 000 cycles and then started to increase after about 2 000 cycles. The initial capacitance decrease maybe ascribed to the existence of heteroatoms, such as oxygen, as confirmed by XPS, which can lead to the pseudocapacitance, and, after a few cycles, fades away after all the heteroatoms have been exhausted [52]. The further increases in the capacitance might be due to the complete wetting of the electrode with the KOH electrolyte. Besides, the swelling of the MFC binder used in this study increases with time and thus leads to a higher amount of ions stored, which, in turn, translates to high capacitance.

3. Conclusions

In summary, a simple and environmentally benign method is proposed for the synthesis of activated graphene-based carbon composites for supercapacitor electrodes. A natural and sustainable material, microfibrillated cellulose (MFC) is used for exfoliation of graphene and as a binder in the electrode fabrication. In comparison to commonly used toxic materials employed for exfoliation of graphene and as binders in supercapacitors, MFC is also biodegradable, renewable and readily available. The optimal graphene concentration for the system was found to be 5 %. At this concentration, a well-developed porosity and a high surface area of 720 $m^2 g^{-1}$ insured an excellent electrochemical behaviour. Besides, the prepared showed a superior cycling stability by retaining 99 % capacitance after 5 000 cycles and 97 % after 10 000 cycles. This type of composite could find significant potential use in advanced applications such as catalysts, energy storage and adsorption.

4. Materials and methods

Materials: Natural graphite flakes were provided by Asbury Carbon. Microfibrillated cellulose was provided by Suzano Pulp and Paper at 5 wt% solids. The MFC was a relatively course grade produced by mechanical defibrillation of hardwood Kraft pulp. The length weighted average fibre length was 0.52 mm measured using a FiberLab laser instrument from Metso Automation. Other properties of MFC can be found in our earlier published work [53]. Deionised water was used throughout the experiments.

Preparation of graphene/MFC suspensions: Co-exfoliation of graphene in MFC suspension was achieved using an IKA Magic Lab micro-plant equipped with a single-walled open 1-dm3 vessel). The MFC was first diluted to a consistency of 0.8 wt%. Subsequently, natural graphite was added to the suspension in various proportions to yield a graphite solid content of 5, 10 and 15 wt% with respect to that of solid MFC. The resulting mixtures were then subjected to high shear exfoliation for 60 min. The same procedure was repeated with 100 % MFC suspension alone. The prepared samples are denoted as G0-0%, G1-5%, G2-10% and G3-15%, where 0, 5, 10 and 15 %, represent the concentration of graphite in the initial production process. The detailed experimental procedure can be found in our earlier publication [29].

After co-exfoliation, excess water from the suspensions was removed by vacuum filtration. The suspensions were then soaked in KOH solution at the mass ratio of 1:1 for 2 h followed by drying in an oven at 105 °C. The dried samples were then activated at 800 °C for 1 h, at a heating rate of 5 °C min^{-1} in nitrogen atmosphere. The yield of pure MFC after carbonization with KOH at a MFC/KOH ratio of 1 was estimated to be around 5 %. The overall yield was around 9.5 %. After carbonisation, the samples were thoroughly washed with HCl and water and subsequently dried for at least 24 h at 105 °C.

Material characterization: The structure of carbonised materials was recorded using a Zeiss Sigma VP scanning electron microscope at 5 kV acceleration voltage. The powders were first sputtered with a gold film before SEM measurements. Raman spectra were measured using a WITec alpha300 R Raman microscope (alpha 300, WITec, Ulm, Germany) equipped with a piezoelectric scanner using a 532 nm linear polarised excitation laser. Surface area and pore volume were determined by nitrogen sorption using a Micromeritics Tristar II by Brunauer-Emmett-Teller (BET) method and Barrett-Joyner-Halenda (BJH) theory, respectively.

Electrochemical measurement: Cyclic voltammetry, galvanostatic charge-discharge, and electrochemical impedance spectroscopy (EIS) measurements were carried out using a Gamry 600+ Reference potentiostat, using a three-electrode cell configuration system. The measurements were conducted in 6 M KOH aqueous electrolyte solution at room temperature. The KOH solution was purged with nitrogen before the experiment. A platinum wire and Ag/AgCl electrode were used as counter and reference electrodes, respectively. The specific capacitance was obtained from galvanostatic charge-discharge using the formula: $C = I\Delta t/(\Delta V m)$, (where, C (F g^{-1}) is specific capacitance, I (A) is discharge current, Δt (s) is discharge time, ΔV (V) is the potential window, and m (g) mass of the active material).

To prepare the electrode, the carbonised materials were directly mixed with MFC suspension, diluted to 1 wt%, to form an electrode consisting of 90 wt% active material and 10 wt% MFC binder. No conductive additives were used. The prepared paste was then coated on a Ni foam and dried in an oven at 105 °C for at least 24 h. The areal mass loading was between 1.5-2 mg cm^{-2}. Before the measurements, the coated Ni foam was pressed at about 7 MPa for 30 s.

Acknowledgements

The authors appreciate financial support from Omya International AG. This work made use of the Aalto University Nanomicroscopy Centre (Aalto-NMC) for SEM imaging and XPS. The authors also appreciate support from Dr. Jouko Lahtinen for conducting the XPS experiments. The authors would also like to extend their appreciation to Asbury Carbons for the supply of free graphite samples.

Received: ((will be filled in by the editorial staff))
Revised: ((will be filled in by the editorial staff))
Published online: ((will be filled in by the editorial staff))

References

[1] J. Chmiola, G. Yushin, Y. Gogotsi, C. Portet, P. Simon, P. L. Taberna, *Science* **2006**, *313*, 1760.

[2] R. Kötz, M. Carlen, *Electrochim. Acta* **2000** *45*, 2483-2498.

[3] J. S. Bonso, A. Rahy, S. D. Perera, N. Nour, O. Seitz, Y. J. Chabal, K. J. Balkus, J. P. Ferraris, D. J. Yang, *J. Power Sources* **2012** *203*, 227-232.

[4] G. A. Snook, P. Kao, A. S. Best, *J. Power Sources* **2011** *196*, 1-12.

[5] Q. Meng, K. Cai, Y. Chen, L. Chen, *Nano Energy* **2017** *36*, 268-285.

[6] C. D. Lokhande, D. P. Dubal, O. Joo, *Curr. Appl. Phys.* **2011** *11*, 255-270.

[7] M. -. Wu, P. -. J. Chiang, *Electrochem. Solid State Lett* **2004**, *7*, A123-A126.

[8] T. Cottineau, M. Toupin, T. Delahaye, T. Brousse, D. Bélanger, *Applied Physics A* **2006**, *82*, 599-606.

[9] L. L. Zhang, R. Zhou, X. S. Zhao, *J. Mater. Chem.* **2010**, *20*, 5983-5992.

[10] Q. Ke, J. Wang, *J of Materiomics* **2016** *2*, 37-54.

[11] G. Wang, L. Zhang, J. Zhang, *Chem. Soc. Rev.* **2012**, *41*, 797-828.

[12] Z. S. Wu, K. Parvez, X. Feng, K. Mullen, *Nat. Commun.* **2013**, *4*, 2487.

[13] Q. Cheng, J. Tang, J. Ma, H. Zhang, N. Shinya, L. Qin, *Phys. Chem. Chem. Phys.* **2011**, *13*, 17615-17624.

[14] Z. S. Iro, C. Subramani, S. Dash, *Int. J. Electrochem. Sci.* **2016**, *11*, 10628-10643.

[15] M. M. Shaijumon, F. S. Ou, L. Ci, P. M. Ajayan, *Chem. Commun.* **2008**, 2373-2375.

[16] K. H. An, W. S. Kim, Y. S. Park, J. Moon, D. J. Bae, S. C. Lim, Y. S. Lee, Y. H. Lee, *Adv. Funct. Mater.* **2001**, *11*, 387-392.

[17] C. Niu, E. K. Sichel, R. Hoch, D. Moy, H. Tennent, *Appl. Phys. Lett.* **1997**, *70*, 1480-1482.

[18] M. F. De Volder, S. H. Tawfick, R. H. Baughman, A. J. Hart, *Science* **2013**, *339*, 535-539.

[19] J. Phiri, P. Gane, T. C. Maloney, *Mater. Sci. Eng. , B* **2017**, *215*, 9-28.

[20] H. A. Becerril, J. Mao, Z. Liu, R. M. Stoltenberg, Z. Bao, Y. Chen, *ACS Nano* **2008**, *2*, 463-470.

[21] Y. Si, E. T. Samulski, *Chem. Mater.* **2008**, *20*, 6792-6797.

[22] C. Liu, Z. Yu, D. Neff, A. Zhamu, B. Z. Jang, *Nano Lett.* **2010**, *10*, 4863-4868.

[23] C. Liu, F. Li, L. Ma, H. Cheng, *Adv Mater* **2010**, *22*, E28-E62.

[24] H. Peng, J. Huang, M. Zhao, Q. Zhang, X. Cheng, X. Liu, W. Qian, F. Wei, *Advanced functional materials* **2014**, *24*, 2772-2781.

[25] B. Huang, L. Peng, F. Yang, Y. Liu, Z. Xie, *Journal of energy chemistry* **2017**, *26*, 712-718.

[26] X. Fan, C. Yu, Z. Ling, J. Yang, J. Qiu, *ACS applied materials & interfaces* **2013**, *5*, 2104-2110.

[27] E. Raymundo- Piñero, M. Cadek, M. Wachtler, F. Béguin, *ChemSusChem* **2011**, *4*, 943-949.

[28] Z. Wu, Y. Sun, Y. Tan, S. Yang, X. Feng, K. Müllen, *J. Am. Chem. Soc.* **2012**, *134*, 19532-19535.

[29] J. Phiri, L. Johansson, P. Gane, T. C. Maloney, *Nanoscale* **2018**, *10*, 9569-9582.

[30] J. Huang, Y. Liang, H. Hu, S. Liu, Y. Cai, H. Dong, M. Zheng, Y. Xiao, Y. Liu, *J. Mater. Chem. A* **2017**, *5*, 24775-24781.

[31] A. Magasinski, P. Dixon, B. Hertzberg, A. Kvit, J. Ayala, G. Yushin, *Nat Mater* **2010**, *9*, 353-358.

[32] J. Wang, S. Kaskel, *J. Mater. Chem.* **2012**, *22*, 23710-23725.

[33] A. Bhatnagar, W. Hogland, M. Marques, M. Sillanpää, *Chem. Eng. J.* **2013** *219*, 499-511.

[34] D. Pan, S. Wang, B. Zhao, M. Wu, H. Zhang, Y. Wang, Z. Jiao, *Chem. Mater.* **2009**, *21*, 3136-3142.

[35] Z. Ni, Y. Wang, T. Yu, Z. Shen, *Nano Res* **2008**, *1*, 273-291.

[36] L. Zhang, Y. Jiang, L. Wang, C. Zhang, S. Liu, *Electrochim. Acta* **2016**, *196*, 189-196.

[37] S. Utsumi, H. Honda, Y. Hattori, H. Kanoh, K. Takahashi, H. Sakai, M. Abe, M. Yudasaka, S. Iijima, K. Kaneko, *J. Phys. Chem. C* **2007**, *111*, 5572-5575.

[38] S. Wang, F. Tristan, D. Minami, T. Fujimori, R. Cruz-Silva, M. Terrones, K. Takeuchi, K. Teshima, F. Rodríguez-Reinoso, M. Endo, *Carbon* **2014**, *76*, 220-231.

[39] K. Xia, Q. Li, L. Zheng, K. You, X. Tian, B. Han, Q. Gao, Z. Huang, G. Chen, C. Zhou, *Microporous and Mesoporous Materials* **2017**, *237*, 228-236.

[40] E. Raymundo-Piñero, K. Kierzek, J. Machnikowski, F. Béguin, *Carbon* **2006** *44*, 2498-2507.

[41] H. Zhou, S. Zhu, M. Hibino, I. Honma, *J. Power Sources* **2003** *122*, 219-223.

[42] M. Yu, X. Cheng, Y. Zeng, Z. Wang, Y. Tong, X. Lu, S. Yang, *Angew. Chem. Int. Ed.* **2016**, *55*, 6762-6766.

[43] H. Xia, Y. S. Meng, G. Yuan, C. Cui, L. Lu, *Electrochemical and Solid-State Letters* **2012**, *15*, A60-A63.

[44] M. Boota, K. Hatzell, E. Kumbur, Y. Gogotsi, *ChemSusChem* **2015**, *8*, 835-843.

[45] L. Li, H. Song, X. Chen, *Electrochim. Acta* **2006** *51*, 5715-5720.

[46] W. Chen, T. Wen, H. Teng, *Electrochim. Acta* **2003** *48*, 641-649.

[47] J. Gamby, P. L. Taberna, P. Simon, J. F. Fauvarque, M. Chesneau, *J. Power Sources* **2001** *101*, 109-116.

[48] X. Du, P. Guo, H. Song, X. Chen, *Electrochim. Acta* **2010**, *55*, 4812-4819.

[49] M. Arulepp, L. Permann, J. Leis, A. Perkson, K. Rumma, A. Jänes, E. Lust, *J. Power Sources* **2004** *133*, 320-328.

[50] Y. Li, T. Shang, J. Gao, X. Jin, *RSC Adv.* **2017**, *7*, 19098-19105.

[51] Y. Kim, B. Lee, H. Suezaki, T. Chino, Y. Abe, T. Yanagiura, K. C. Park, M. Endo, *Carbon* **2006**, *44*, 1592-1594.

[52] C. Shi, L. Hu, K. Guo, H. Li, T. Zhai, *Adv. Sustainable Syst.* **2017**, *1*, 1600011.

[53] J. Phiri, L. Johansson, P. Gane, T. Maloney, *Compos. Part B: Engin.* **2018** *147*, 104-113.

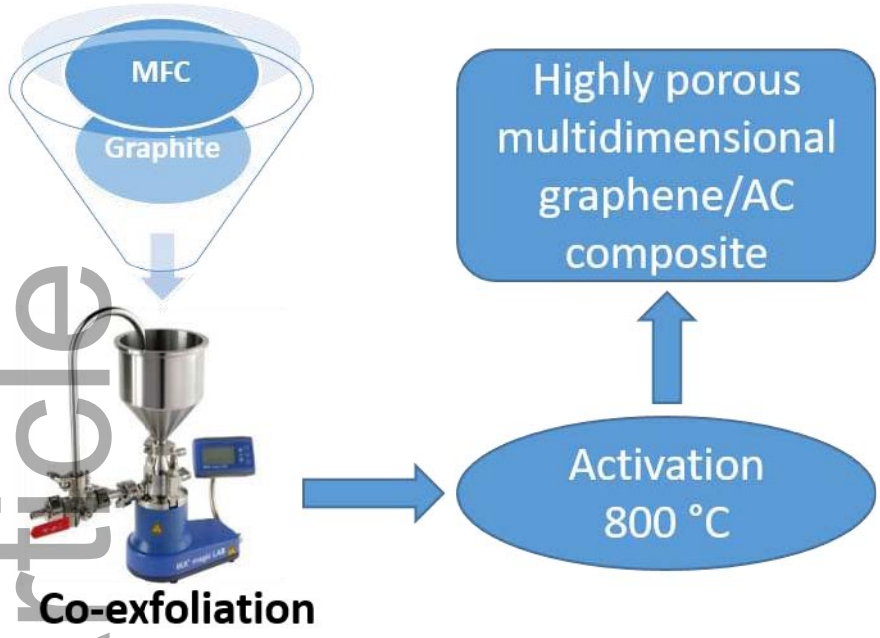

Figure 1 schematic representation of the fabrication process of graphene/AC composites

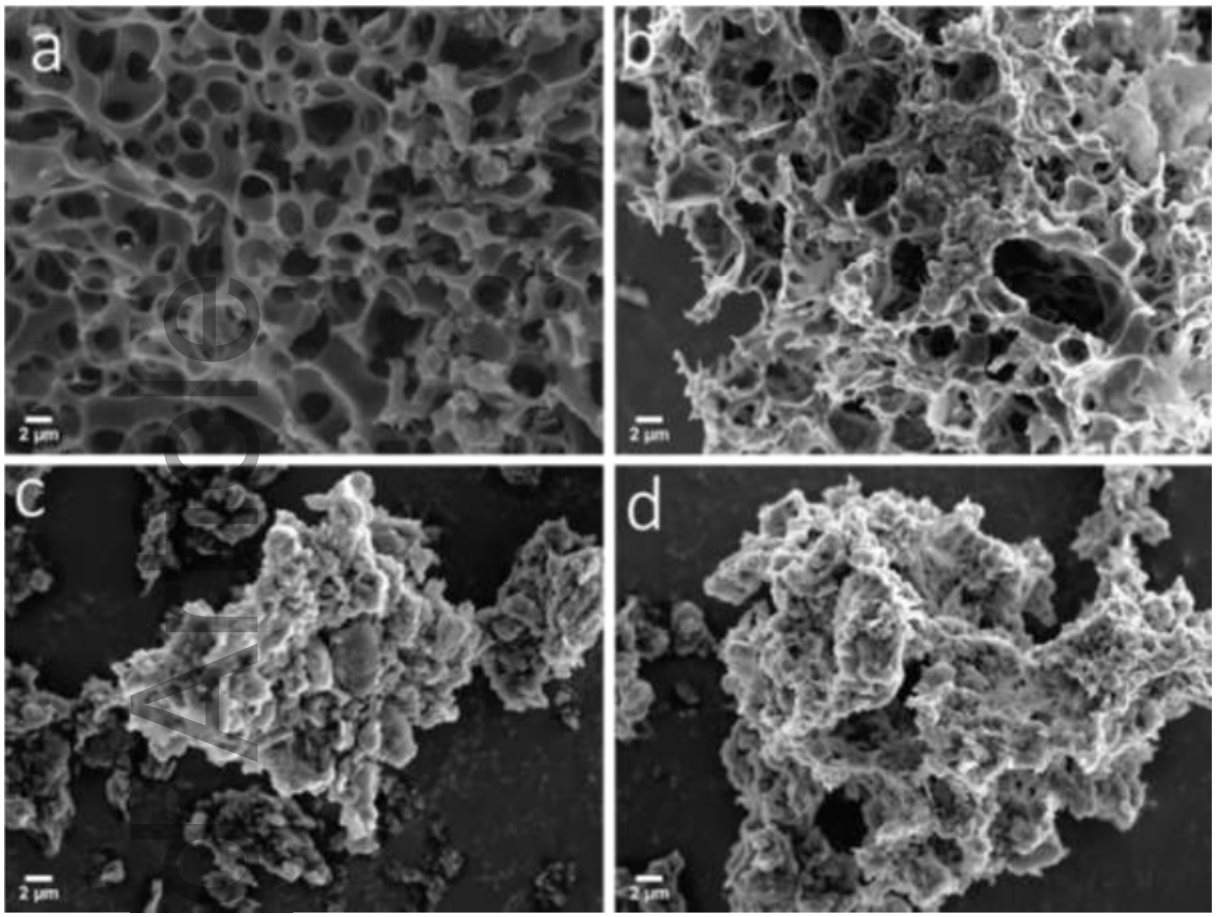

Figure 2 SEM images showing the morphologies of the synthesised samples (a) G0-0%; (b) G1-5%; (c) G2-10%; (d) G3-15%

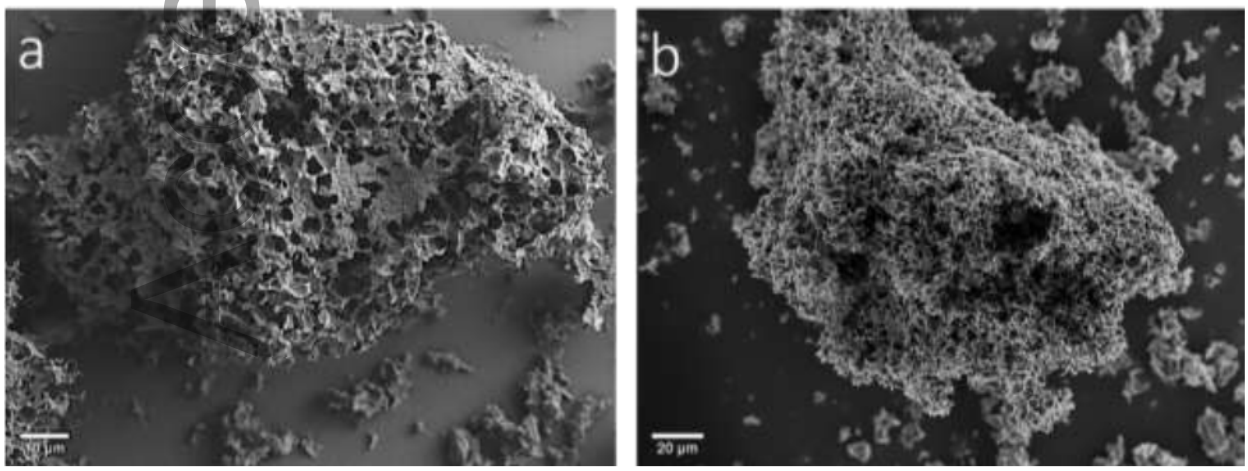

Figure 3 SEM images of G1-5% at different resolutions showing a more pronounced 3-dimensional structure.

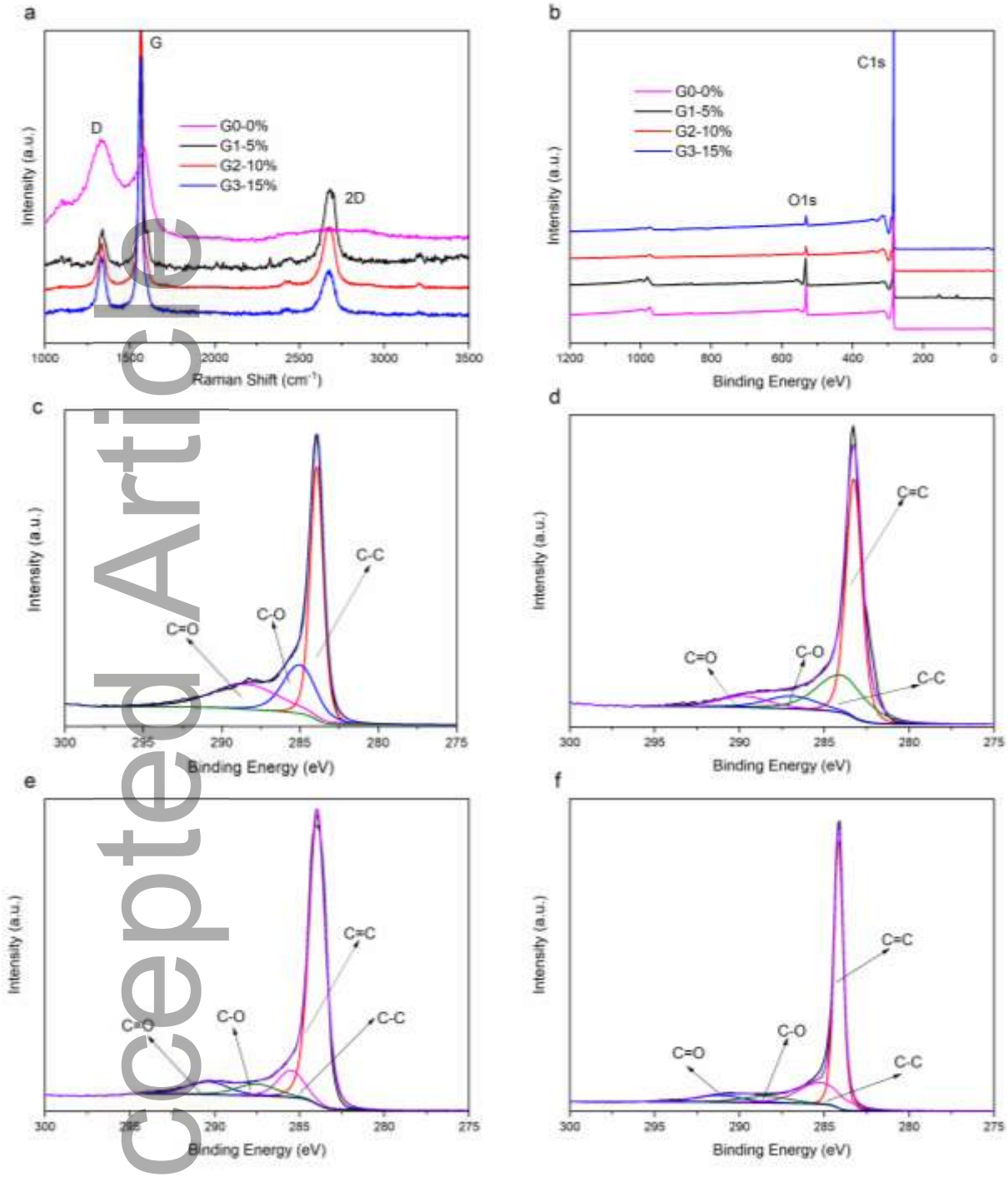

Figure 4 (a) Normalised Raman spectra for the prepared samples showing the presence of all typical bands; (b) Wide XPS survey spectra. High resolution C1s XPS spectra of G0-0% (c), G1-5% (d), G2-10% (e) and G3-15% (f).

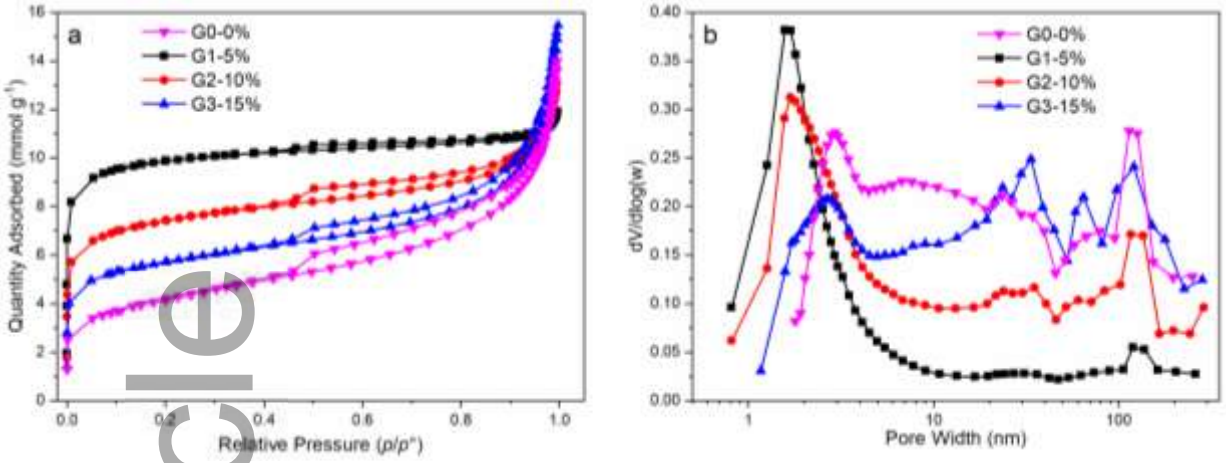

Figure 5 Pore structure characterisation of the samples: (a) Nitrogen adsorption-desorption isotherms; (b) pore size distribution

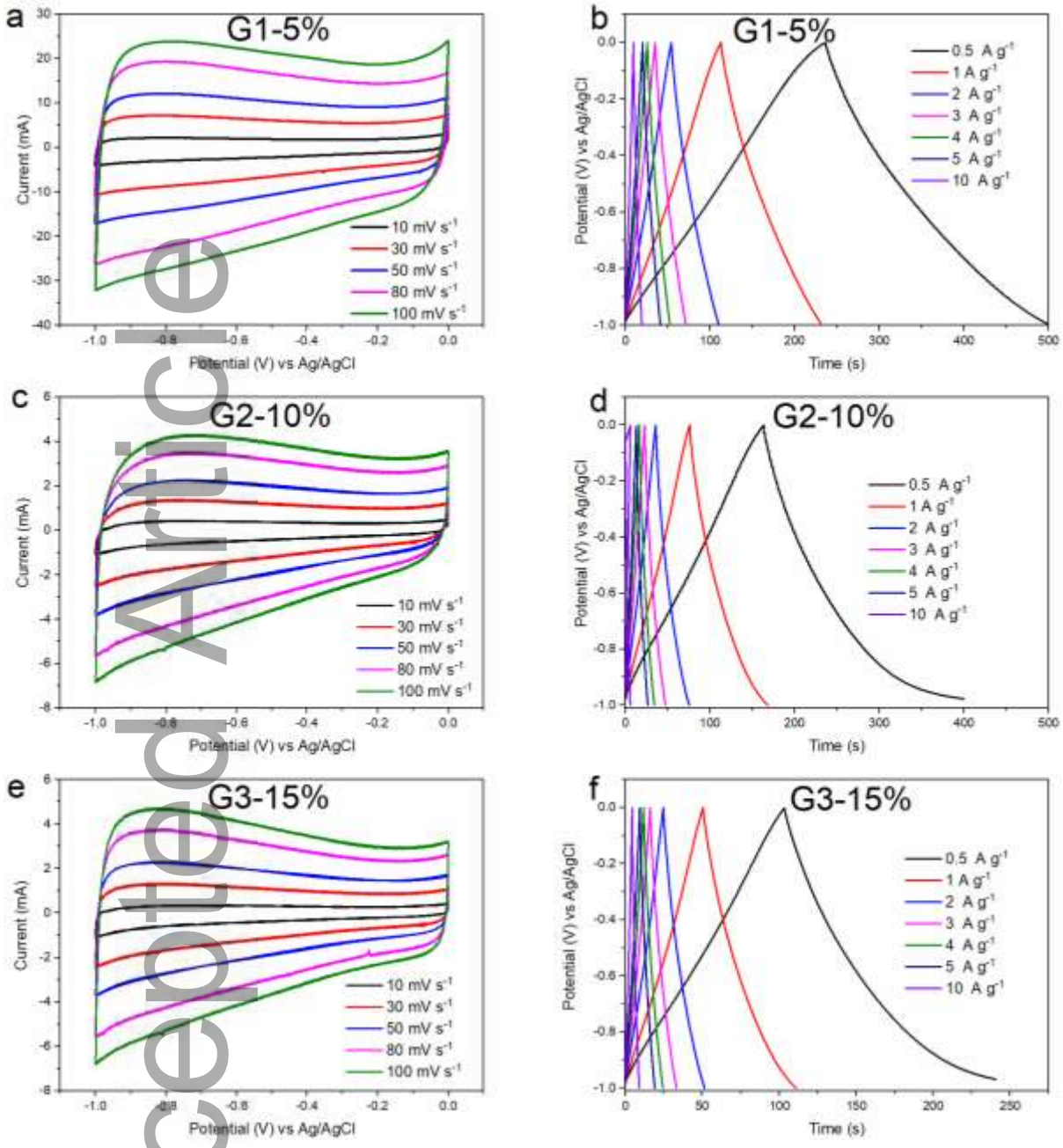

Figure 6 Electrochemical evaluation of the samples: (a), (c) and (d) the cyclic voltammetry curves at different scan rates and (b), (d) and (f) the galvanostatic charge/discharge cycles at various current densities ranging from 0.5 to 10 A g^{-1}.

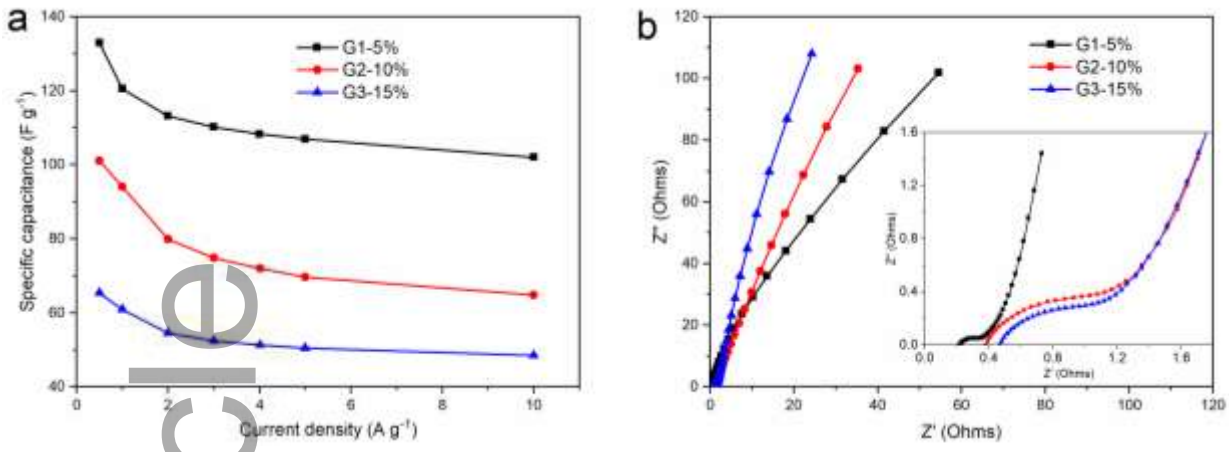

Figure 7 (a) Specific capacitance as a function of current density and (b) Nyquist plots showing the imaginary part versus the real part of impedance with the insert showing the magnification of the high-frequency region

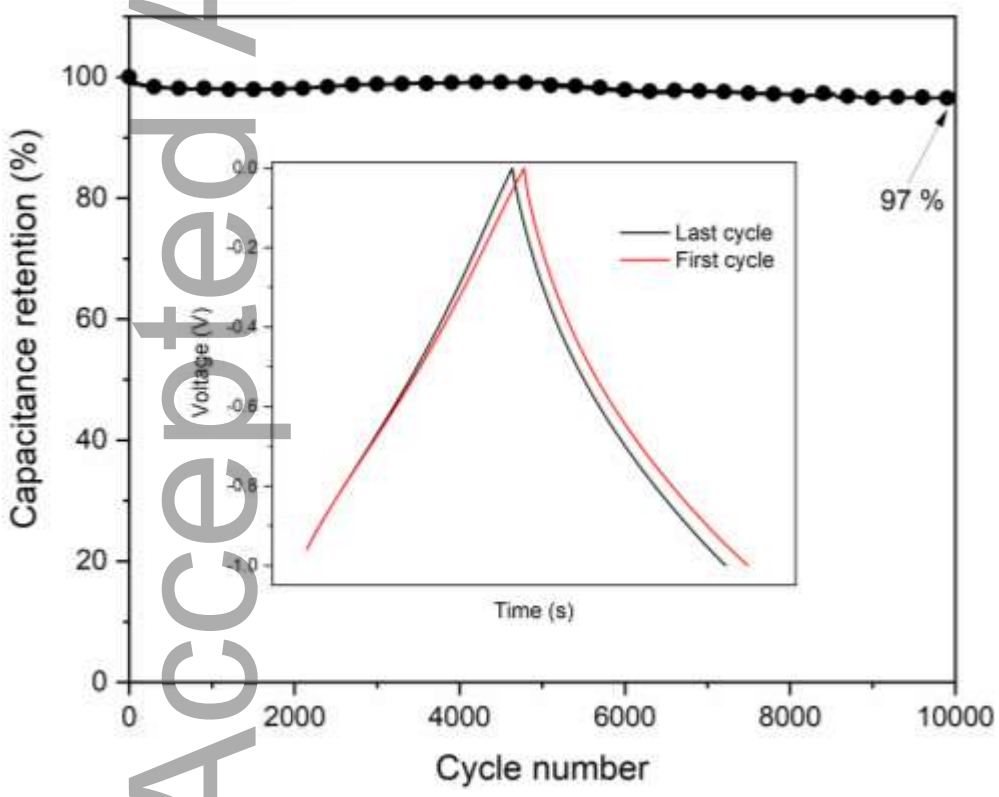

Figure 8 Cycling stability tests of the best performing sample G1-5% at a current density of 5 A g^{-1}; the insert shows the charge-discharge cycles at different intervals

Table 1 Average $I_{D/G}$ value and XPS chemical composition of the samples

Samples	$I_{D/G}$	Composition, (at. %)	
		C	O
G0-0%	0.864	88.4	11.0
G1-5%	0.147	81.0	14.7
G2-10%	0.153	96.8	2.9
G3-15%	0.201	97.3	2.2

Table 2 Porosity characteristics of the samples and specific capacitance at the current density of 1 A g^{-1}

Samples	BET, $m^2 g^{-1}$	Pore volume, $cm^3 g^{-1}$	Average pore width, nm	Specific capacitance, F g^{-1}
G0-0%	314	0.42	8.2	15
G1-5%	720	0.24	1.8	120
G2-10%	546	0.35	3.1	94
G3-15%	424	0.42	6.5	61

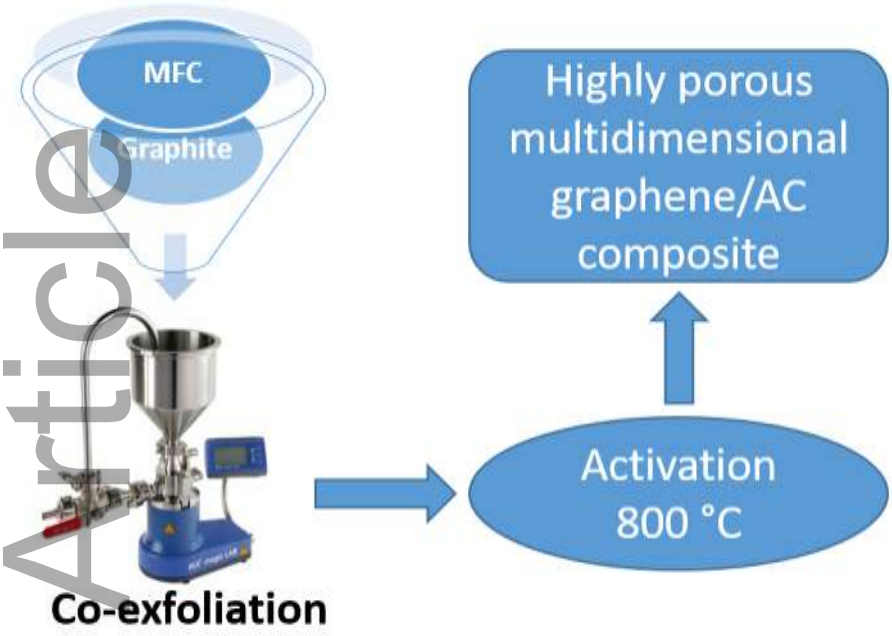

A simple method for fabrication of graphene based hybrid electrodes for energy storage application is presented. This method can serve as route for fabrication of high performance, energy storage devices based largely on renewable and sustainable materials with a potential for large-scale application.